Case Studies in Construction Materials 18 (2023) e02104

Contents lists available at ScienceDirect

Case Studies in Construction Materials

journal homepage: www.elsevier.com/locate/cscm

Full length article

# Mechanical behavior in terms of shear and bending performance of reinforced concrete beam using waste fire clay as replacement of aggregate

Yasin Onuralp Özkılıç [a,*], Boğaçhan Başaran [b], Ceyhun Aksoylu [c], Memduh Karalar [d], Carlos Humberto Martins [e,*]

[a] Faculty of Engineering, Department of Civil Engineering, Necmettin Erbakan University, Konya, Turkey
[b] Vocational School of Technical Sciences, Department of Construction, Amasya University, Amasya, Turkey
[c] Faculty of Engineering and Natural Sciences, Department of Civil Engineering, Konya Technical University, Turkey
[d] Faculty of Engineering, Department of Civil Engineering, Zonguldak Bulent Ecevit University, Zonguldak, Turkey
[e] Department of Civil Engineering, State University of Maringá, Brazil

ARTICLE INFO

*Keywords:*
Recycled
Waste
Beam
Reinforced concrete
Shear
Bending
Flexural
Fire clay
Aggregate
ACI 318

ABSTRACT

In this experimental and analytical study, waste fire clay (WFC) was consumed by the use of replacing fine aggregate (FA) in confident amounts. It is targeted to remove the current sustainable complications by confirming the consumption of WFC in reinforced concrete beams (RCBs) as raw materials. For this purpose, FAs were partially replaced with WFC in proportions of 0 %, 10 %, 20 %, and 30 %. Based on this motivation, a series of experimental studies were performed on 12 + 12 small-scale bending and shear RCBs of 100×150×1000mm, considering altered WFC and stirrup spacing. While the percentage of WFC in the RCBs was selected as 0 %, 10 %, 20 %, and 30 % by weight, correspondingly, the longitudinal reinforcement was taken into account as Φ12, Φ10, Φ8. Besides, while the longitudinal tension and compression reinforcements of constant 2Φ12 and 2Φ6, the stirrup spacing was chosen as 160 mm, 200 mm, and 270 mm. As a result of the study, increasing the tensile reinforcement ratio has made the WFC less effective. Similarly, as stirrup spacing decreases, stirrup dominates the behavior, and as stirrup spacing increases, WFC determines the behavior. Finally, while the WFC content for bending RCBs increases the ability at the maximum level for the range of 20 %−30 %, it can be said that the optimum WFC content for shear RCBs is 20 %. The experimental results were obtained with the prediction of ACI-318 and the reason for the difference between the expected and actual values can be explained in detail.

## 1. Introduction

Fireclay (FC) is a type of clay that is highly resistant to heat and used in various industrial and construction applications. FC is one of the most favourable and widely used insulating and construction resources in manufacturing productivity. It has gained this popular definition as a results of its high thermal shock endurance, high heat endurance, and high abrasion endurance belongings [1]. Therefore, it is often used to produce firebricks, which line fireplaces, furnaces, and other high-temperature applications. It is also used

* Corresponding authors.
*E-mail addresses:* yozkilic@erbakan.edu.tr (Y.O. Özkılıç), chmartins@uem.br (C.H. Martins).

https://doi.org/10.1016/j.cscm.2023.e02104
Received 14 March 2023; Received in revised form 8 April 2023; Accepted 24 April 2023
Available online 25 April 2023

to make refractory materials designed to withstand extremely high temperatures without degrading. When its structural belongings are observed, it is realized that it contains 50–60 % silica and 18–44 % alumina [2]. In addition to its heat resistance, FC is also known for its durability and resistance to chemical corrosion. Therefore, it is often used to produce ceramics, such as dinnerware and bathroom fixtures, due to its ability to hold its shape and withstand exposure to water and other liquids.

Waste of fireclay (WFC) is generated during the production of FC products, such as firebricks and refractory materials. This waste can include broken or unusable pieces of fireclay products and waste generated during the manufacturing process, such as trimming or cutting scraps. Disposing of WFC can be challenging, as it is a heavy and bulky material that is not easily biodegradable. Manufacturers and scientific specialists have established several kinds of investigation to reprocess manufacturing garbage as an additional substantial for several manufacturing requests corresponding to heat-resisting bricks, concrete, plastics, iron manufacture, etc. [3–16]. This exchange decreases the manufacturing industry's raw material price and recycles unused material [17–32]. There is an inadequate investigation related to FC products in the literature. One of these studies was performed by İssi et al. [33]. Their study observed fine fire clay's investigative forming and sintering performance, which has an altered subdivision dimension collated with raw resources [33]. At the end of this study, it was established that consuming two particle dimensions distribution in the FC arrangement was more operational than the one particle-sized arrangement. Joyklad et al. [34] performed an investigational study to observe the influence of consuming brick waste in concrete as a substitution for natural coarse aggregates. For this purpose, coarse aggregates obtained from bricks were gained by crushing fired clay bricks. Two substitution percentages of coarse brick aggregates were considered as 50 % and 100 % to investigate the influence of the coarse brick aggregates concrete containing density, compression strength (CS), tensile splitting, modulus of elasticity, and stress-strain behaviour, which were made of natural aggregates. After the investigation, it was observed that the strength-related belongings of brick aggregates (BAs) concrete reduced as the ratio of clay brick (CB) aggregates improved in the concrete combination. Miah et al. [35] performed another study to investigate the mechanical behaviour of BA on concrete. In this study, Miah et al. [35] detected that the concrete prepared with BA has considerably worse mechanical strength and more excellent permeability than conventional concrete. Furthermore, SEM analysis of BA and concrete designed with fired clay BA presented that BAs contain more spaces and cracks. Other investigational studies also described that coarse aggregates prepared from the fired clay bricks had the eventuality to be expended to generate material of comprehensible quality [36, 37]. The other experimental study was performed by Miah et al. [38]. In this study, Miah et al. [38] considered the flexural and stability acts of RCBs prepared with initiation furnace steel slag aggregate as a substitution for fired clay BA.

Zheng et al. [39] examined the effect of hardened concrete on CSs. For this purpose, the natural coarse aggregate was replaced with reprocessed concrete aggregate (RCA) or reprocessed clay brick aggregate (RBA). It has been carefully advanced using RCA and RBA optimum degradation in concrete mixes to increase the performance of the recovered aggregates. In general, it was observed in this study that concrete with RCA had improved performance than concrete with RBA. The other experimental analysis was performed by Ibrahim et al. [40]. In this study, Ibrahim et al. [40] defined the belongings and features of lightweight foam concrete consuming waste CB as an alternate substantial to decrease the reduction of raw aggregate. Four altered proportions of concrete combinations consuming raw aggregate have been organized for this aim. Zhang et al. [41] investigated the implementation of fibers on concrete with reused aggregates prepared from crushed CB. For this aim, a relative investigation was achieved on the mechanical and permanence belongings of concrete prepared with CB as coarse aggregates and with raw aggregates.

As can be realized from the literature studies above, a few investigations have been performed on the mechanical properties of WFC. However, besides these studies, it is realized that there are no experimental studies on beam bending and shear behaviour of the reinforced concrete beams using WFC. The primary goal of this experimental and analytical investigation is to determine the influence of WFC material in altered percentages on the bending and shear behaviour of the RCB. The details of the study will be given in the following sections.

## 2. Material methods

To perform the retainable concrete, cement (CEM I 32.5) was consumed with specific percentages of fine aggregates (FA) and coarse aggregates integrated with WFC for mechanical strength. The reused concrete combination aimed to attain the most operational combination that encounters necessities with optimal waste resources. For this purpose, weights of 0 %, 10 %, 20 %, and 30 % of FA were exchanged with WFC (Fig. 1).

The design of the concrete used in the experiment is presented in Table 1. Prepared samples were experienced under compression and splitting tensile tests. At least three samples were tested to determine the mechanical belongings of concrete. To determine the

**Fig. 1.** WFC.

compression strength (CS) of the maintainable concrete with WFC, 150 × 150 × 150 mm cubic samples were used. At the end of these tests, the average CS of 22.0 MPa, 23.3 MPa, 25.3 MPa, and 22.7 MPa was obtained for the concrete with 0 %, 10 %, 20 %, and 30 % WFC. The converted cylinder CS is 17.7, 20.4, 18.8 and 18.3 MPa, respectively. Furthermore, splitting tensile tests were performed using 100 × 200 mm cylindrical test samples. The average splitting tensile strength of 2.10 MPa, 2.25 MPa, 2.29 MPa, and 2.19 MPa was found for the concrete with 0 %, 10 %, 20 %, and 30 % WFC. The slump values were detected as 18 cm, 14 cm, 11 cm and 8 cm for concrete with 0 %, 10 %, 20 %, and 30 % WFC, respectively. This indicates that workability decreases as the amount of WFC increases.

Three parameters were chosen to investigate the RCBs: the WFC ratio, the amount of longitudinal reinforcement, and stirrups. Experiments were performed separately for shear and bending RCBs. All beam specimens had a length of 1000 mm and cross-sections of 100 × 150 mm. A total of 24, including 12 shear and 12 bending half-scale RCBs, were prepared. Three specimens were used as a reference sample without WFC, both shear and bending RCBs. The stirrups were designated constant Φ6/100 mm to gain the bending performance. In specimens, the longitudinal tension reinforcements of 2Φ12, 2Φ10, and 2Φ8 were used. Detailed information on the bending beam specimens is given in Table 2.

To observe the influence of the shear behaviour of RCBs, altered stirrup spacing having RCBs was tested. For this purpose, while the longitudinal tension and compression reinforcements of constant 2Φ12 and 2Φ6, the stirrup spacing was chosen as 160 mm, 200 mm, and 270 mm. Furthermore, quantities of WFC are selected as the weight of 0 %, 10 %, 20 %, and 30 %. Detailed information on the shear beam specimens is given in Table 3.

The numbers for S27, S20, and S16 indicate spacing of the stirrups of 270 mm, 200 mm, and 160 mm, respectively. The typical reinforcement layout utilized in the bending and shear RCBs is given in Fig. 2. Additionally, the specimen test setup containing a servo-controlled hydraulic is demonstrated in Fig. 3.

## 3. Experimental consequences and discussion

In this section, bending and shear RCBs are observed in detail. First, bending RCBs are detailed, then shear RCBs are explained, and comparisons are performed.

### 3.1. Influence of different longitudinal reinforcement on WFC

In order to observe the influence of altered longitudinal reinforcements, bending RCBs were established with altered longitudinal reinforcements. The reference RCBs are symbolized via FC, and the WFC additional RCBs are characterized via FC0 %. For example, RCB Φ12_FC0 % means an RCB with a WFC constituent of 0 % and a longitudinal reinforcement used as Φ12. Correspondingly, Φ12_FC10 % characterizes an RCB using a WFC substance of 10 % and a longitudinal reinforcement used as Φ12. Detailed information is given in subsequent divisions.

#### 3.1.1. Case 1: rupture and load-bending behaviour of RCB (Φ12_FC0 %, Φ10_FC0 %, Φ8_FC0 %, Φ12_FC10 %, Φ10_FC10 %, Φ8_FC10 %)

The influence of altered amounts of longitudinal reinforcement on rupture and descent forms of the RCBs is observed in altered amounts of WFC. For this target, quantities of longitudinal reinforcement are chosen as Φ12, Φ10 and Φ8, while WFC in the RCB is selected regularly as 0 %. As presented in Fig. 4, the load–displacement curves of the RCB tests presented and the crack and descent arrangements of the RCBs were detected. As presented in Fig. 4, for the longitudinal reinforcement chosen as Φ12, the maximum load level was found as 72.67 kN, and the maximum displacement was obtained as 26.01 mm. While the longitudinal reinforcement was selected as Φ10, these values were obtained as 49.65 kN and 49.52 mm. As the longitudinal reinforcement decreased to Φ8, it was attained that these values reduced until 37.82 kN and 42.42 mm. While the influence of longitudinal reinforcement on the load-deformation capabilities of RCBs is detected, as estimated, as the longitudinal reinforcement decreases, the load-deformation capabilities of the RCBs gradually decrease as a consequence of the forthcoming existence of shear cracks in the RCBs. In other words, The load-carrying ability of Φ12_FC0 % was 46.3 % and 92.1 % higher than Φ10_FC0 % and Φ8_FC0 %, respectively. This situation also caused the RCBs to behave more ductile by decreasing the amount of tensile reinforcement. Damage views of the specimens at the end of the experiment are presented in Fig. 5.

On the other hand, WFC in the RCB is designated as 10 % while quantities of longitudinal reinforcement are chosen as Φ12, Φ10, and Φ8 to investigate the influence of altered amounts of longitudinal reinforcement on rupture and descent forms of the RCBs. As presented in Fig. 4, the load–displacement curves of the RCB offered, and the crack and descent arrangements of the RCBs are noticed. As noticed in Fig. 4, for the longitudinal reinforcement selected as Φ12, the maximum load level was obtained as 75.55 kN, and the maximum displacement was saved as 20.71 mm. While the longitudinal reinforcement was designated as Φ10, these values were found

**Table 1**
Combination of the concrete.

| Mixture (ratio) | Cement (kg) | Water (kg) | Fine Aggregate (kg) | Coarse Aggregate (kg) | Fire-Clay Waste (kg) |
|---|---|---|---|---|---|
| 0 % | 580 | 270 | 780 | 900 | 0 |
| 10 % | | | 702 | | 78 |
| 20 % | | | 624 | | 156 |
| 30 % | | | 546 | | 234 |

**Table 2**
Properties of the bending specimens.

| # | Name | Compression | Tensile | aρ | $w_f$ |
|---|---|---|---|---|---|
| 1 | Φ12_FC0 % | 2ϕ6 | 2ϕ12 | 0.0174 | 0 % |
| 2 | Φ10_FC0 % | | 2ϕ10 | 0.0121 | |
| 3 | Φ8_FC0 % | | 2ϕ8 | 0.0077 | |
| 4 | Φ12_FC10 % | 2ϕ6 | 2ϕ12 | 0.0174 | 10 % |
| 5 | Φ10_FC10 % | | 2ϕ10 | 0.0121 | |
| 6 | Φ8_FC10 % | | 2ϕ8 | 0.0077 | |
| 7 | Φ12_FC20 % | 2ϕ6 | 2ϕ12 | 0.0174 | 20 % |
| 8 | Φ10_FC20 % | | 2ϕ10 | 0.0121 | |
| 9 | Φ8_FC20 % | | 2ϕ8 | 0.0077 | |
| 10 | Φ12_FC30 % | 2ϕ6 | 2ϕ12 | 0.0174 | 30 % |
| 11 | Φ10_FC30 % | | 2ϕ10 | 0.0121 | |
| 12 | Φ8_FC30 % | | 2ϕ8 | 0.0077 | |

[a] $\rho$ is the tensile reinforcement ratio ($A_s/b_w d$).

**Table 3**
Properties of shear specimens.

| # | Name | Stirrups Diameter/Spacing | Volumetric ratio of stirrups ($\rho_w$) % | $w_f$ % |
|---|---|---|---|---|
| 1 | S27_FC0 % | Φ6/270 | 2.1 | 0 |
| 2 | S20_FC0 % | Φ6/200 | 2.8 | 0 |
| 3 | S16_FC0 % | Φ6/160 | 3.53 | 0 |
| 4 | S27_FC10 % | Φ6/270 | 2.1 | 10 |
| 5 | S20_FC10 % | Φ6/200 | 2.8 | 10 |
| 6 | S16_FC10 % | Φ6/160 | 3.53 | 10 |
| 7 | S27_FC20 % | Φ6/270 | 2.1 | 20 |
| 8 | S20_FC20 % | Φ6/200 | 2.8 | 20 |
| 9 | S16_FC20 % | Φ6/160 | 3.53 | 20 |
| 10 | S27_FC30 % | Φ6/270 | 2.1 | 30 |
| 11 | S20_FC30 % | Φ6/200 | 2.8 | 30 |
| 12 | S16_FC30 % | Φ6/160 | 3.53 | 30 |

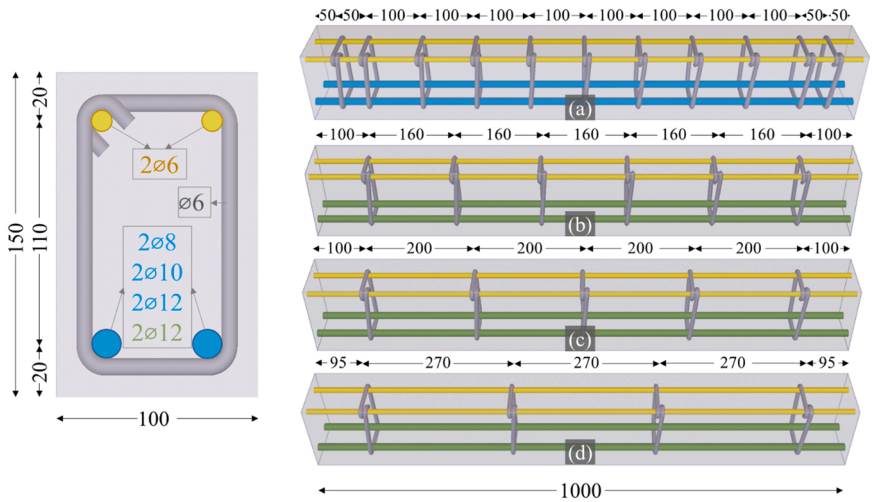


**Fig. 2.** a) The typical reinforcement layout utilized in the bending and shear RCBs for 2Φ12, 2Φ10, 2Φ8; The reinforcement stirrup spacing b) 160 mm, c) 200 mm, d) 270 mm (All dimensions in mm).

as 52.77 kN and 60.01 mm. As the longitudinal reinforcement reduced to Φ8, it was reached that these values reduced until 41.26 kN and 62.00 mm. As can be realized from the load-displacement graph in Fig. 4, the load-carrying ability of the RCB increases as the WFC ratio rises. This increase varies with reference samples with no WFC. Toward from Φ12 to Φ8 tensile reinforcement, the rate of increase was 3.9 %, 6.2 %, and 9.0 %, respectively. This shows that WFC contributes more to the load-carrying ability as the tensile reinforcement ratio decreases. Besides, WFC contributed to the ductility of all specimens. However, a decrease in deformation ability was observed on only Φ12_FC10 %. Therefore, shear damage was observed in the Φ12_FC10 % sample. Furthermore, as presented in Fig. 5,

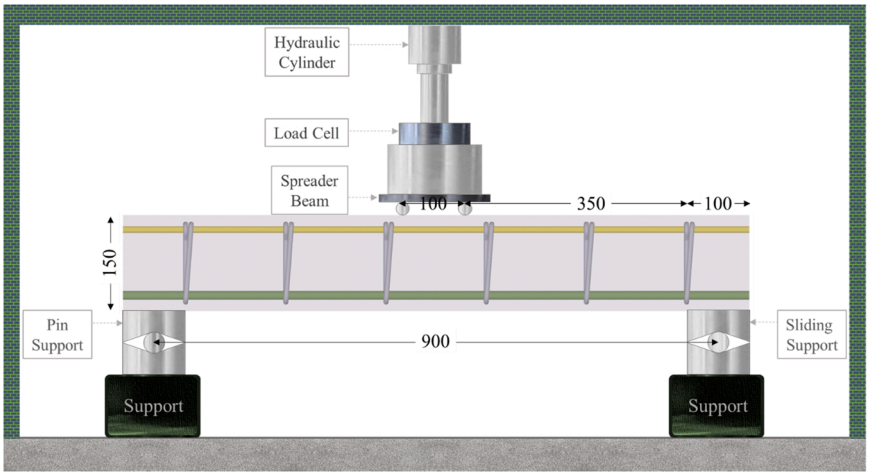


**Fig. 3.** Investigational Test setup (All dimensions in mm).

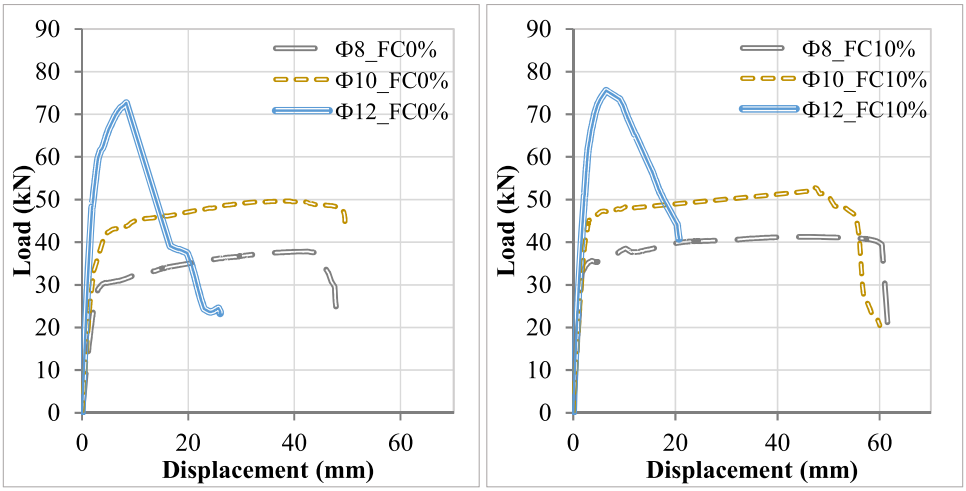


**Fig. 4.** Load-displacement view of test specimens for Φ12_FC0 %, Φ10_FC0 %, Φ8_FC0 %.

as the longitudinal tensile reinforcement diameter increased, the rupture pattern changed from flexural crack to shear crack type.

*3.1.2. Case 2: rupture and load-bending behaviour of RCB (Φ12_FC20 %, Φ10_FC20 %, Φ8_FC20 %, Φ12_FC30 %, Φ10_FC30 %, Φ8_FC30 %)*

WFC in the RCB is chosen as 20 % as quantities of longitudinal reinforcement are selected as Φ12, Φ10, and Φ8. As presented in Fig. 6, the load–displacement figures of the RCB tests presented in the study and the crack and descent arrangements of the RCBs are observed. As observed in Fig. 6, for the longitudinal reinforcement designated as Φ12, the maximum load level was recognized as 77.40 kN, and the maximum displacement was recognized as 21.42 mm. While the longitudinal reinforcement was selected as Φ10 and Φ8, these values were found as 55.80 kN-50.32 mm and 41.82 kN-66.56 mm, respectively. As can be realized from the load-displacement graph in Fig. 6, the load-carrying ability of the RCB increases as the WFC ratio rises. However, a decrease in deformation ability is observed. Furthermore, as can be recognized from Fig. 7, as the longitudinal reinforcement diameter increased, the rupture pattern changed from flexural crack to shear crack type. In other words, typical bending behavior depending on ductility was observed in Φ10_FC20 % and Φ8_FC20 % specimens, while Φ12_FC20 % specimen provided sufficient ductility up to the maximum load, but after this load, it suffered shear damage and collapsed. As the tensile reinforcement diameter decreased from Φ12 to Φ8 (for 20 % WFC), the load-carrying ability increased by 6.5 %, 12.3 %, and 10.5 % over the reference sample. This increase is more significant than the increase in RCBs with a WFC content of 10 %. In addition, specimens with 20 % WFC content improved ductility collated to the reference specimens. However, the ductility was obtained lower than the specimen with 10 % WFC content with tensile reinforcement Φ8.

On the other hand, WFC in the RCB is selected as 30 % as quantities of longitudinal reinforcement are chosen as Φ12, Φ10, and Φ8. In Fig. 6, the load–displacement views of the RCB tests are presented, and the crack and descent arrangements of the RCBs are detected.

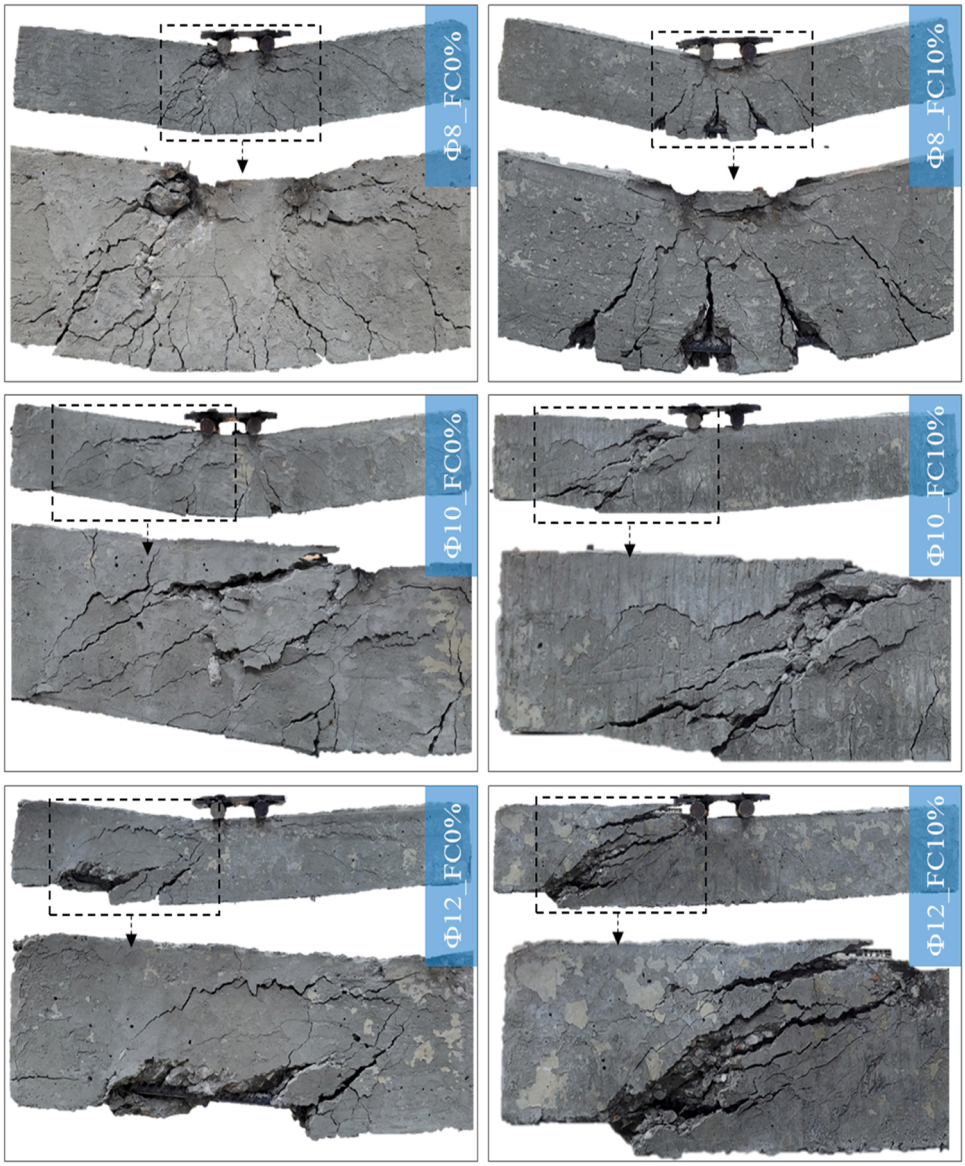


**Fig. 5.** Collapse view of test specimens for Φ8_FC0 %, Φ10_FC0 %, Φ12_FC0 %, Φ8_FC10 %, Φ10_FC10 %, Φ12_FC10 %.

As detected in Fig. 6, for the longitudinal reinforcement designated as Φ12, the maximum load level was recognized as 76.55 kN, and the maximum displacement was recognized as 23.12 mm. While the longitudinal reinforcement was selected as Φ10 and Φ8, these values were found as 54.22 kN-44.62 mm and 42.18 kN-64.44 mm, respectively. Collated to the reference sample (Φ12_FC0 %, Φ10_FC0 %, Φ8_FC0 %), toward from Φ12 to Φ8 tensile reinforcement, the rate of increase was 5.3 %, 9.2 %, and 11.5 %, respectively. In addition, 30 % contribution of WFC contributed to all samples' ductility except for Φ12 reinforced samples. However, its contribution to the load-carrying ability was not as much as 20 % WFC. As presented in Fig. 7, ductile behavior was observed in the specimens. However, shear damage was also observed after the ductile behavior was observed in the Φ12_FC30 % sample. This occurred after reaching the load-carrying ability.

*3.1.3. Case 3: rupture and load-bending attitude of a proportion of WFC for longitudinal reinforcement as Φ8, Φ10, Φ12*

WFC was selected as 0 %, 10 %, 20 %, and 30 %, while longitudinal reinforcement in the RCB was selected continuously as Φ8, Φ10, and Φ12. There were notable bending cracks in the RCB depending on the vertical load, as presented in Fig. 8. In Fig. 8, collated to the reference specimen (Φ8_FC0 %), the load-carrying ability increased amid 9 % and 11.5 % in the specimen with WFC additives. The stiffness values at the point of yielding (0.85 $P_{max}$) increased amid 28.4 % and 147.3 % collated to the reference specimen. The increase in the ductility value varied amid 66.1 % and 336.9 % collated to the reference specimen. As the percentage of the WFC improved from 0 % to 30 %, the load-deformation capabilities of the RCBs progressively improved as a result of the future existence of shear cracks in

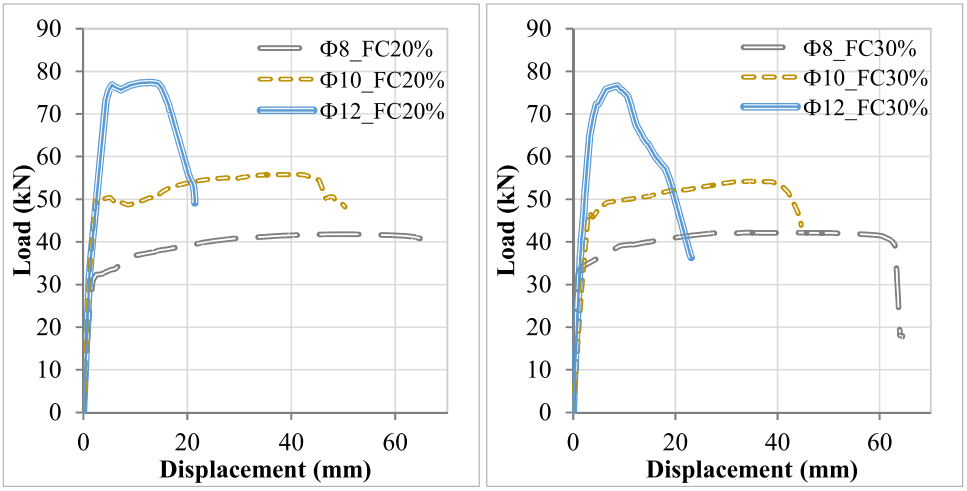


**Fig. 6.** Load-displacement view of test specimens for Φ12_FC20 %, Φ10_FC20 %, Φ8_FC20 %, Φ12_FC30 %, Φ10_FC30 %, Φ8_FC30 %.

the RCBs, as presented in Fig. 9.

Concerning Fig. 10, collated to the reference specimen (Φ10_FC0 %) without WFC additives, increases of 6.2–12.3 % occurred. The stiffness values at the point of yielding (0.85 $P_{max}$) increased amid 60.6 % and 147.4 % collated to the reference specimen. The increase in the ductility value varied amid 40 % and 108.3 % collated to the Φ10_FC0 % specimen. Flexural damage occurred significantly in beam specimens with 20 % and 30 % WFC percentages. In Fig. 11, the end-of-experiment damages of the specimens are presented.

In relation to Fig. 12, for Φ12_FC0 % reference specimen, the maximum load level was increased to 72.67 kN, and the maximum displacement was obtained as 26.01 mm. Specimens with WFC additives increased amid 3.9 % and 6.5 % collated to the Φ12_FC0 % reference specimen. As the tensile reinforcement ratio increases, the beam bending ability increases. Therefore, the shear ability becomes more effective in determining the load-carrying ability. Increasing the tensile reinforcement ratio has made the WFC less effective. For sufficient ductility of RCBs with sub-balance, the ductility ratio should be 4–5. However, the ductility ratio of Φ12_FC0 % and Φ12_FC10 % specimens were obtained as 3.01 and 3.85, respectively. Therefore, after partially bending behavior, the ultimate damage occurred as shear. The ductility percentages of Φ12_FC20 % and Φ12_FC30 % specimens were obtained as 4.72 and 4.11, respectively. After sufficient ductility was observed in these RCBs, shear damage occurred. In Fig. 13, the end-of-experiment damages of the specimens are illustrated.

The alterations in load, displacement, stiffness, ductility, and energy dissipation abilities gained from investigational studies are presented in Tables 4 and 5.

### *3.1.4. Comparison of bending test consequences with ACI 318 Codes*

In the study, the bending strengths of RCBs were calculated using the equivalent stress block method and conformity equations recommended in the ACI 318–19 regulation to determine the maximum bending strength of RCBs (Fig. 14). In this context, the maximum strain ($\varepsilon_{cu}$) in the outermost fiber of the concrete was taken as 0.003. The modulus of elasticity ($E_s$ and $E_s'$) of tensile and compression reinforcements is 200,000 MPa, and the yield strengths ($f_y$) are 560, 550, 510 and 500 MPa for 6, 8, 10 and 12 mm diameter reinforcements, respectively.

where $b_w$ is the width of beam, $h$ is height of beam, $d$ is effective height. In the calculations, the equivalent pressure block depth ($a$) of the beam was calculated by Eqs. 4 and 5 using the conformity equations (Eqs. 1 and 2) and the equilibrium equations (Eq. 3), since all RCBs are equipped under balance. The so-called (nominal) moment capacities ($M_n$) of the RCBs are calculated using Eqs. 6 and 7. The consequences calculated by the equivalent stress block method and the experimental consequences are presented in Table 6. Differences up to 16 % were found amid the experimental and theoretical bearing capacities of the RCBs.

$$\frac{\varepsilon_{cu}}{c} = \frac{\varepsilon_s}{d-c} \tag{1}$$

$$\frac{\varepsilon_{cu}}{c} = \frac{\varepsilon_s{}'}{c-d'} \tag{2}$$

$$F_s = F_c + F_s' \tag{3}$$

$$a = \frac{A_s f_y + A_s'\left(\varepsilon_{cu} E_s' \frac{c-d'}{c}\right)}{0.85 f_c' b_w} \varepsilon_s{}' \leq \varepsilon_y{}' \tag{4}$$

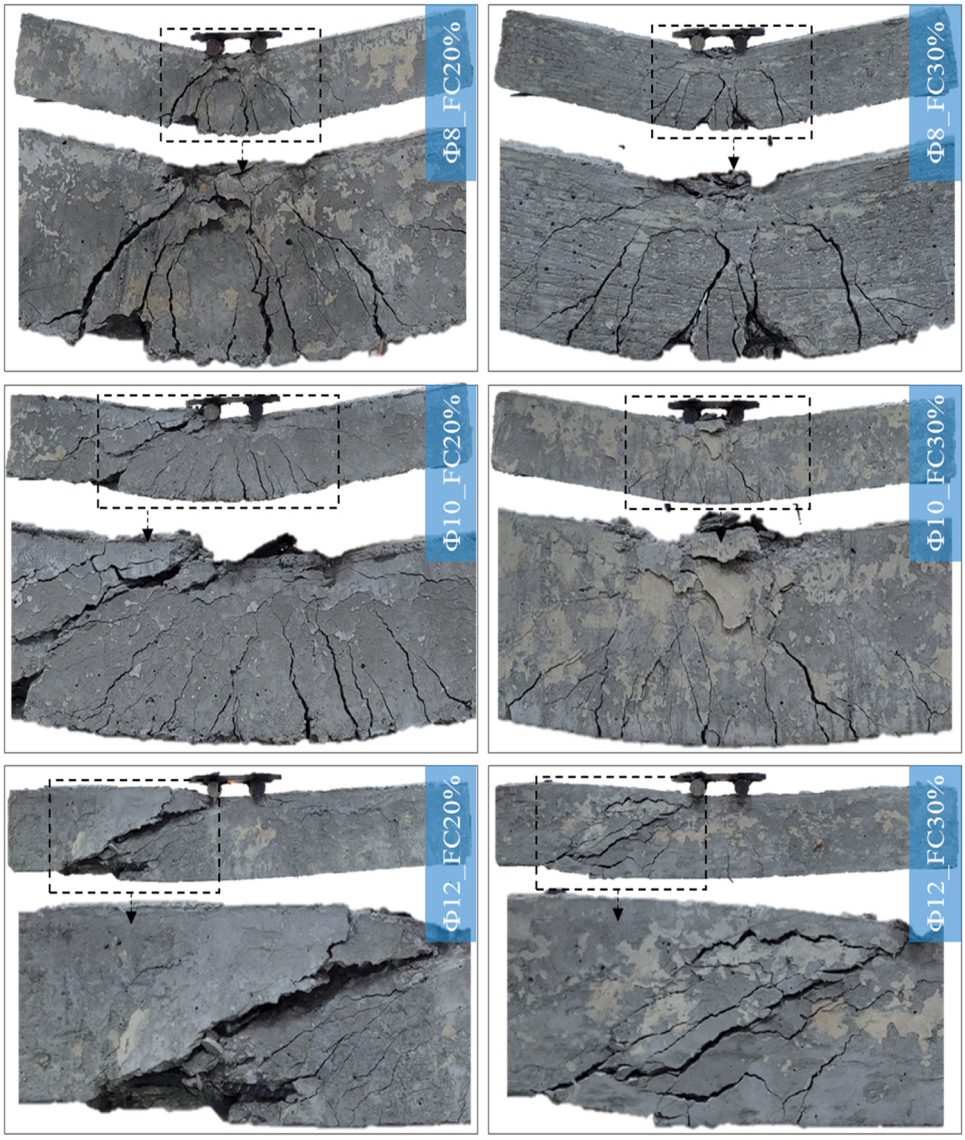


**Fig. 7.** Collapse view of test specimens for Φ12_FC20 %, Φ10_FC20 %, Φ8_FC20 %, Φ12_FC30 %, Φ10_FC30 %, Φ8_FC30 %.

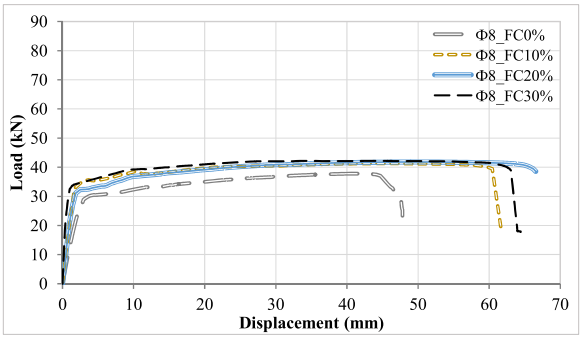


**Fig. 8.** Comparison of load displacement of RCBs with Φ8 longitudinal reinforcement for a altered amount of WFC.

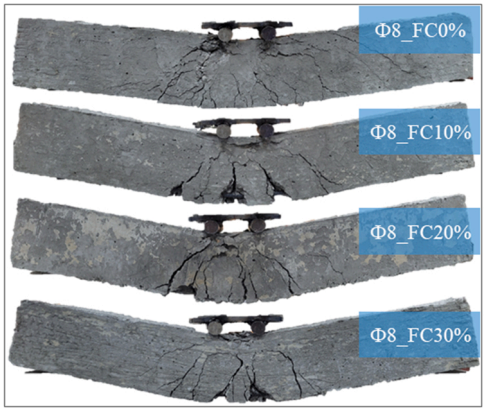


**Fig. 9.** Collapse view of test specimens for Φ8_FC0 %, Φ8_FC10 %, Φ8_FC20 %, Φ8_FC30 %.

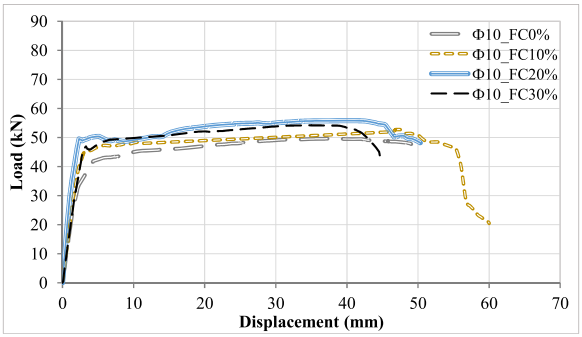


**Fig. 10.** Comparison of load displacement of RCBs with Φ10 longitudinal reinforcement for a altered amount of WFC.

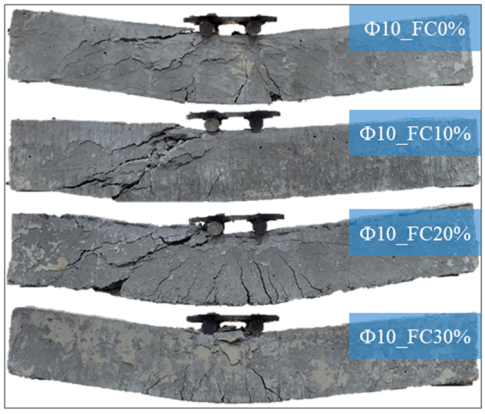


**Fig. 11.** Collapse view of test specimens for Φ10_FC0 %, Φ10_FC10 %, Φ10_FC20 %, Φ10_FC30 %.

$$a = \frac{A_s f_y + A_s' f_y'}{0.85 f_c' b_w} \varepsilon_s' > \varepsilon_y' \tag{5}$$

$$M_n = A_s f_y \left(d - \frac{a}{2}\right) + A_s' \left(\varepsilon_{cu} E_s' \frac{c - d'}{c}\right) \left(\frac{a}{2} - d'\right) \varepsilon_s' \leq \varepsilon_y' \tag{6}$$

$$M_n = A_s f_y \left(d - \frac{a}{2}\right) + A_s' f_y' \left(\frac{a}{2} - d'\right) \varepsilon_s' > \varepsilon_y' \tag{7}$$

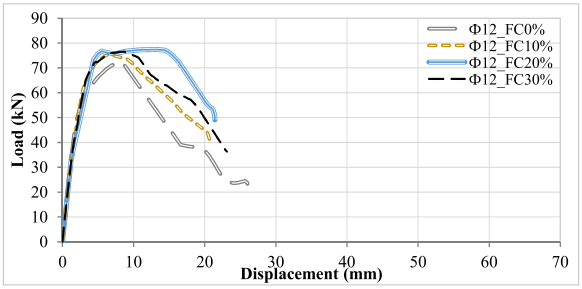


**Fig. 12.** Comparison of load displacement of RCBs with Φ12 longitudinal reinforcement for a altered amount of WFC.

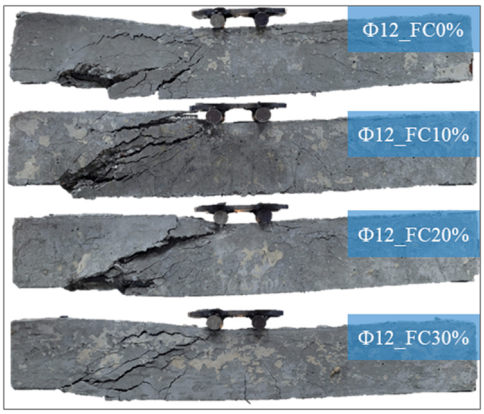


**Fig. 13.** Collapse view of test specimens for Φ12_FC0 %, Φ12_FC10 %, Φ12_FC20 %, Φ12_FC30 %.

**Table 4**
Experimental consequences for load and displacement values.

| Test specimens | $P_{max}$ (kN) | Displacement at $P_{max}$ (mm) | Stiffness at ($P_{max}$) (kN/mm) | $P_u$ (0.85$P_{max}$) (kN) | Displacement at Yield $\delta_y$ (mm) | Stiffness at Yield (kN/mm) | $\delta_u$ (mm) | Ductility ratio |
|---|---|---|---|---|---|---|---|---|
| Φ12_FC0 % | 72.67 | 8.32 | 8.73 | 61.76 | 3.65 | 16.88 | 11.01 | 3.01 |
| Φ10_FC0 % | 49.65 | 38.18 | 1.30 | 42.21 | 4.73 | 8.90 | 49.52 | 10.44 |
| Φ8_FC0 % | 37.82 | 42.42 | 0.89 | 32.14 | 9.62 | 3.34 | 46.58 | 4.84 |
| Φ12_FC10 % | 75.55 | 6.44 | 11.71 | 64.22 | 3.25 | 19.71 | 12.55 | 3.85 |
| Φ10_FC10 % | 52.77 | 47.38 | 1.11 | 44.86 | 3.02 | 14.30 | 55.53 | 18.36 |
| Φ8_FC10 % | 41.26 | 46.29 | 0.89 | 35.07 | 2.86 | 12.22 | 60.70 | 21.15 |
| Φ12_FC20 % | 77.40 | 13.04 | 5.93 | 65.79 | 3.79 | 17.35 | 17.89 | 4.72 |
| Φ10_FC20 % | 55.80 | 41.20 | 1.35 | 47.43 | 2.15 | 22.02 | 46.86 | 21.75 |
| Φ8_FC20 % | 41.82 | 48.96 | 0.85 | 35.54 | 8.27 | 4.29 | 66.56 | 8.04 |
| Φ12_FC30 % | 76.55 | 8.65 | 8.84 | 65.07 | 3.26 | 19.95 | 13.41 | 4.11 |
| Φ10_FC30 % | 54.22 | 34.72 | 1.56 | 46.09 | 3.02 | 15.24 | 44.22 | 14.62 |
| Φ8_FC30 % | 42.18 | 33.95 | 1.24 | 35.85 | 4.33 | 8.26 | 63.20 | 14.57 |

*At yield is 0.85$P_{max}$ point.

There was a maximum difference of 10 % and an average of 5 % amid the experimental consequences and the theoretical consequences of the RCBs using non-FC admixture. This difference is due to the neglect of tensile stiffness (hardening) in the steel reinforcement in the theoretical calculation. As the use of FC in RCBs increased, the difference amid experimental and theoretical consequences widened slightly. The mean difference was 10 % in 10 % FC usage, 12.3 % in 20 % FC usage and 12.7 % in 30 % FC usage.

However, if the 5 % hardening difference in the theoretical calculation of FC-doped RCBs is neglected, the main difference can be more accurately determined in FC-doped RCBs. In this context, the average difference increased to 5 % in 10 % FC usage, 7.3 % in 20 % FC usage, and 7.7 % in 30 % FC usage. Therefore, the FS of FC reinforced RCBs can be determined with at least 5 % more confidence with the equivalent stress block method.

All beams in this series are designed so that once they reach their bending moment capacity ($M_{n,ACI}$), the shear force demanded from the beam ($V_{Mmax}$) is lower than the beam's shear capacity ($V_n$ according to Eq. 10) (in Table 6). Therefore, bending failure was expected in all beams in this series. However, although the theoretical shear capacities of the samples with Φ12 longitudinal

**Table 5**
Experimental test consequences for energy dissipation capacities.

| Test specimens | Maximum Displacement (mm) | Energy Dissipation at $P_{max}$ (kJ) | Energy Dissipation at *0.85* $P_{max}$ (kJ) | Plastic Energy Dissipation (kJ) | Total Energy Dissipation (kJ) | Collapse type | Ductility level |
|---|---|---|---|---|---|---|---|
| Φ12_FC0 % | 26.01 | 0.931 | 0.161 | 1.064 | 1.225 | Bending+Shear | Deficient |
| Φ10_FC0 % | 49.52 | 1.760 | 0.175 | 2.091 | 2.266 | Bending | Sufficient |
| Φ8_FC0 % | 47.81 | 1.438 | 0.276 | 1.340 | 1.617 | Bending | Sufficient |
| Φ12_FC10 % | 20.71 | 0.545 | 0.140 | 1.082 | 1.222 | Bending+Shear | Deficient |
| Φ10_FC10 % | 60.01 | 2.28 | 0.088 | 2.715 | 2.803 | Bending | Sufficient |
| Φ8_FC10 % | 62.00 | 1.792 | 0.072 | 2.334 | 2.406 | Bending | Sufficient |
| Φ12_FC20 % | 21.42 | 0.866 | 0.205 | 1.211 | 1.416 | Bending+Shear | Sufficient |
| Φ10_FC20 % | 50.32 | 2.142 | 0.067 | 2.545 | 2.612 | Bending | Sufficient |
| Φ8_FC20 % | 66.56 | 1.886 | 0.254 | 2.352 | 2.607 | Bending | Sufficient |
| Φ12_FC30 % | 23.12 | 0.523 | 0.135 | 1.246 | 1.381 | Bending+Shear | Sufficient |
| Φ10_FC30 % | 44.62 | 1.717 | 0.091 | 2.134 | 2.225 | Bending | Sufficient |
| Φ8_FC30 % | 64.44 | 1.382 | 0.327 | 2.261 | 2.588 | Bending | Sufficient |

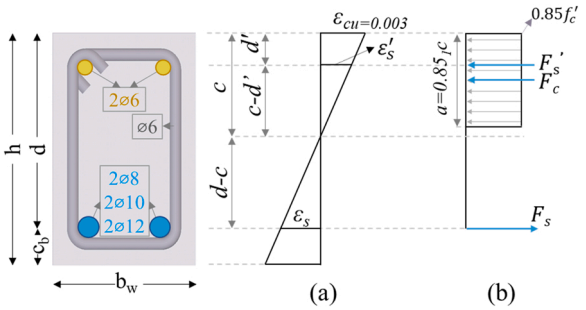


**Fig. 14.** Crack behavior of test specimens.

**Table 6**
Comparison of experimental consequences with ACI 318–19.

| Exp. | $M_{n,ACI}$ (kNm) | $M_{Exp.}$ (kNm) | $M_{Exp./ACI}$ (kNm) | $V_{Mmax}$ (kN) | $V_n$ (kN) | Exp. | $M_{n,ACI}$ (kNm) | $M_{Exp.}$ (kNm) | $M_{Exp./ACI}$ (kNm) | $V_{Mmax}$ (kN) | $V_n$ (kN) |
|---|---|---|---|---|---|---|---|---|---|---|---|
| Φ12_FC0 % | 11.59 | 12.72 | 1.10 | 33.11 | 45.43 | Φ12_FC20 % | 11.90 | 13.55 | 1.14 | 34.00 | 48.81 |
| Φ10_FC0 % | 8.80 | 8.69 | 0.99 | 25.16 | 44.36 | Φ10_FC20 % | 8.94 | 9.77 | 1.09 | 25.54 | 47.66 |
| Φ8_FC0 % | 6.34 | 6.62 | 1.04 | 18.10 | 43.22 | Φ8_FC20 % | 6.40 | 7.32 | 1.14 | 18.30 | 46.43 |
| Φ12_FC10 % | 11.72 | 13.22 | 1.13 | 33.49 | 46.80 | Φ12_FC30 % | 11.66 | 13.40 | 1.15 | 33.32 | 46.17 |
| Φ10_FC10 % | 8.86 | 9.23 | 1.04 | 25.32 | 45.69 | Φ10_FC30 % | 8.84 | 9.49 | 1.07 | 25.25 | 45.09 |
| Φ8_FC10 % | 6.36 | 7.22 | 1.13 | 18.18 | 44.51 | Φ8_FC30 % | 6.35 | 7.38 | 1.16 | 18.15 | 43.92 |

reinforcement ($\rho = 0.0174$) were designed at least 37 % more than the demanded shear force, these beams could not reach their bending capacity, and shear bending failure occurred in the beams at a level close to reaching their bending capacity.

### *3.2. Experimental investigation of shear behavior of RCBs*

In this part of the study, to observe the influence of the shear behavior of RCBs, altered stirrup spacing having RCBs was tested. When the behavior of RCBs without shear reinforcement is observed, there are five altered forms of collapse produced as a result of diagonal cracks depending on the sizes, geometries, type of loading, quantity of longitudinal reinforcement, and structural features of concrete participants. The collapse arrangements are diagonal tension collapse, shear compression/tension collapse, web crushing collapse, and arch rib collapse. On the other hand, in RCBs with stirrup, diagonal tension (DT) collapse or shear compression (SC) collapse is observed in RCBs with an *a/d* ratio of approximately 2.5. In addition, It is known that SC collapse is less brittle than DT. While evaluating the collapse analysis of all RCBs, the conditions at the time of damage were considered. The collapse pattern photos show the condition after the damage. This study, the stirrup spacing was chosen as 160 mm, 200 mm, and 270 mm. Furthermore, quantities of WFC are chosen as 0 %, 10 %, 20 %, and 30 %. Then, the following sections compared the shear behavior.

#### *3.2.1. Case 1: rupture and load-bending attitude of RCB (S16_FC0 %, S20_FC0 %, S27_FC0 %, S16_FC10 %, S20_FC10 %, S27_FC10 %)*

This section first observed the WFC content of 0 %. The load–displacement curves of the RCB tests are presented in Fig. 15. For the

stirrup spacing selected as 160 mm, the maximum load level was found as 70.54 kN, and the maximum displacement was obtained as 15.79 mm. While the stirrup spacing was selected as 200 mm, these values were obtained as 62.17 kN and 12.84 mm. As the stirrup spacing improved to 270 mm, it was found that these values decreased until 54.00 kN and 10.97 mm. Fig. 16 shows that all RCBs have collapsed with SC collapse except for S27_FC0 %. Specimen S27_FC0 % has reached collapse with DT. Breaking was observed in specimen S27_FC0 % due to the leverage influence. In addition, at the same time, the influence of stirrup positioning on the load-deformation capabilities of RCBs is observed. As expected, as the stirrup spacing reduces, the load-deformation abilities of the RCBs gradually increase as a result of the future existence of shear cracks in the RCBs.

Secondly, the WFC ratio, including 10 %, was chosen as a substitution for cement to observe the influences of WFC percentages with stirrup spacing on shear behaviour. As offered in Fig. 15, for the stirrup spacing selected as 160 mm, the maximum load level was found as 75.48 kN, and the maximum displacement was observed as 15.24 mm. While the stirrup spacing was selected as 200 mm, these values got 66.86 kN and 14.27 mm. As the stirrup spacing improved to 270 mm, it was found that these values reduced until 59.54 kN and 6.37 mm. DT collapse occurred in these RCBs with 10 % WFC content (Fig. 16). Breaking was also observed in specimen S27_FC0 % due to the leverage influence. Additionally, while the influence of stirrup positioning on the load-deformation abilities of RCBs is detected as estimated, as the stirrup spacing decreases, the load-deformation abilities of the RCBs increasingly grow. Namely, the load carrying ability of Φ27_FC10 %, Φ20_FC10 %, Φ16_FC10 % examples increased by 10.2 %, 7.5 % and 7 %, respectively, collated to Φ27_FC0 %, Φ20_FC0 %, Φ16_FC0 % examples. In addition, the load-carrying ability of the Φ16_FC10 % specimen increased by 26.7 % and 12.9 %, respectively, collated to the Φ27_FC10 % and Φ20_FC10 % specimens.

### *3.2.2. Case 2: rupture and load-bending attitude of RCB (S16_FC20 %, S20_FC20 %, S27_FC20 %, S16_FC30 %, S20_FC30 %, S27_FC30 %)*

In this section, WFC, including 20 % were swapped as a substitution for FA to observe the influences of WFC with stirrup spacing on shear behavior. As presented in Fig. 17, for the stirrup spacing selected as 160 mm, the maximum load level was found as 78.50 kN, and the maximum displacement was realized as 20.27 mm. While the stirrup spacing was selected as 200 mm, these values were 72.97 kN and 18.49 mm. As the stirrup spacing improved to 270 mm, it was found that these values reduced till 66.87 kN and 12.40 mm. The load-carrying ability of the Φ16_FC20 % specimen increased by 17.4 % and 7.5 %, respectively, collated to the Φ27_FC20 % and Φ20_FC20 % specimens. The load-carrying ability of the Φ16_FC20 % specimen was 11.2 % and 4 % higher than the Φ16_FC0 % and Φ16_FC10 % specimens, respectively. Similarly, the load-carrying ability of the Φ20_FC20 % and Φ27_FC20 % specimens were 17.3 %−9.1 % and 23.8 %−12.3 higher than the Φ20_FC0 %- Φ20_FC10 % and Φ27_FC0 %- Φ27_FC10 % specimens, respectively. It is understood that as stirrup spacing decreases, stirrup dominates the behavior, and as stirrup spacing increases, WFC determines the behavior. When the shear damage types in the specimens were observed, SC collapse was observed at Φ16_FC20 %, while the other two specimens reached the collapse mode with DT (Fig. 19). In addition, the ductility ratio of Φ20_FC20 % and Φ16_FC20 % specimens were obtained as 3.99 and 3.90. It can be stated that 20 % WFC contributes also improves ductility.

When the WFC included 30 %, changes in the mechanical Belongings of the beam were observed. As presented in Fig. 17, the load–displacement curves of the RCB tests were collated. Based on these curves, for the stirrup spacing selected as 160 mm, 200 mm, and 270 mm, the maximum load level was found as 77.14 kN, 66.84 kN, and 60.16 kN, respectively. Maximum displacement values were obtained as 22.52 mm, 17.76 mm, and 10.85 mm, respectively. The load-carrying ability of the Φ16_FC30 % specimen increased by 28.2 % and 15.4 %, respectively, collated to the Φ27_FC30 % and Φ20_FC30 % specimens. The load-carrying ability of the Φ16_FC30 %, Φ20_FC30 % and Φ27_FC30 % specimens were 1.6–8.4 % - 10 % lower than the Φ16_FC20 %, Φ20_FC20 % and Φ27_FC20 % specimens, respectively. In other words, except %30 WFC contributes, the higher the ratio of WFC, the greater the increase in load-carrying ability. As the spacing of the stirrups in the RCB reduced (270 mm > 200 mm>160 mm), the WFC also had a positive influence on the bearing ability of the RCB at increasing WFC values (0 %<10 %<20 %<30 %) (Fig. 18). The aim for this might be presented that the portion of shear stresses protected by the stirrup is higher due to the decrease of the stirrup spacing. Furthermore, as revealed above, while the influence of stirrup spacing on the load-bearing capabilities of RCBs is detected, as the stirrup spacing decreases, the load-bearing capabilities of the RCBs progressively increase as a consequence of the later existence of shear cracks in the RCBs. When the shear damage types in the specimens were observed, DT collapse was observed at Φ16_FC30 %, Φ20_FC30 %, and Φ27_FC30 % specimens (Fig. 19). In addition, the ductility ratio of Φ20_FC30 % specimen was obtained as 3.96. It can be stated that only Φ20_FC30 % specimen improves ductility.

### *3.2.3. Case 3: Rupture and load-bending attitude of a proportion of WFC for stirrup spacing of 160 mm, 200 mm, and 270 mm*

The amounts of WFC ratio are selected as 0 %, 10 %, 20 %, and 30 % while stirrup spacing in the RCB is selected continuously as 160 mm. As detected by examination consequences for 0 %, 10 %, 20 %, and 30 %, it is inspected that only for Φ16_FC20 % specimens were notable bending cracks depending on the vertical load as offered in Fig. 20 and Fig. 21. According to the Fig. 20, the load-carrying ability of the Φ16_FC20 % specimen was 11.2 %, 4 %, and 1.76 % higher than the Φ16_FC0 %, Φ16_FC10 %, Φ16_FC30 % specimens, respectively. This indicates that 20 % of WFC ratio additive is optimal for load-bearing ability. In Fig. 21, SC collapse was observed in Φ16_FC0 % and Φ16_FC20 % specimens, while DT collapse was observed in Φ16_FC10 % and Φ16_FC30 % specimens.

For continuously selected stirrup specimens as 200 mm in Fig. 22, The Φ20_FC20 % specimen presented an increase in load-carrying ability amid 9.1 % and 17.3 %. The ductility ratio for Φ20_FC20 % and Φ20_FC30 % specimens is quite close to the 4–5 range required for typical bending RCBs. As related to these conditions, it might be discovered that as the ratio of the WFC improved from 0 % to 30 %, the load-deformation competencies of the RCBs increasingly improved until the 20 % WFC ratio. In other words, this indicates again that 20 % of WFC ratio additive is optimal for load-bearing ability. When Fig. 23 is observed, SC collapse was observed in Φ20_FC0 % specimen, and DT collapse was observed in Φ20_FC10 %, Φ20_FC20 %, and Φ20_FC30 % specimens.

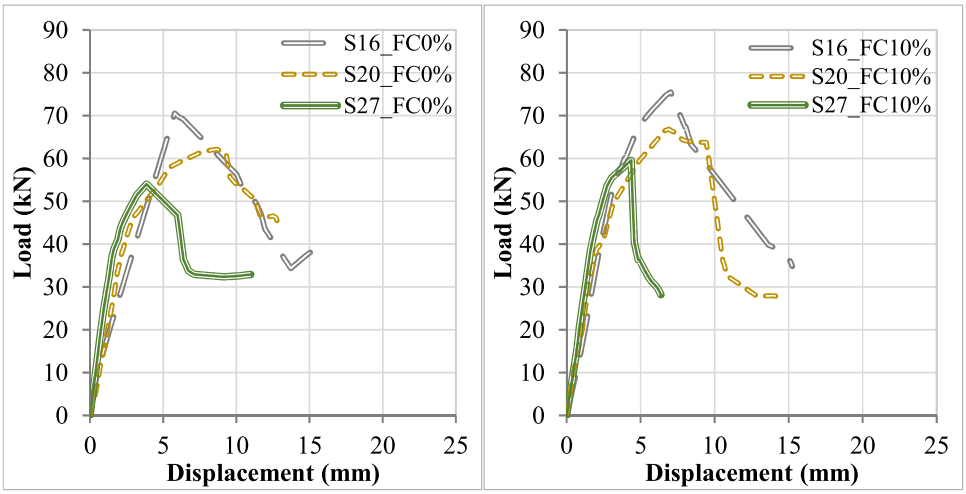


**Fig. 15.** Comparison of load displacement of RCBs for 0 % and 10 % WFC ratio with stirrup spacing; a) 160 mm, b) 200 mm, c) 270 mm.

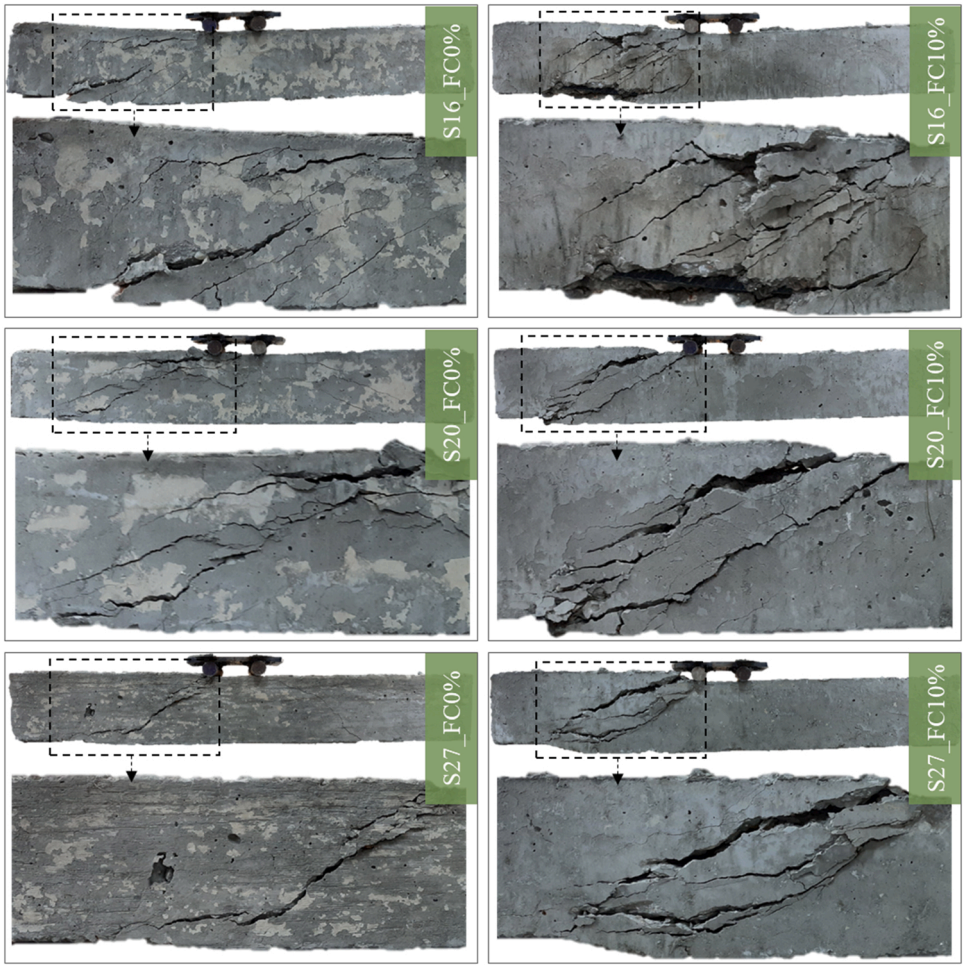


**Fig. 16.** Comparison of collapse patterns for 0 % and 10 % WFC ratio with stirrup spacing; a) 160 mm, b) 200 mm, c) 270 mm.

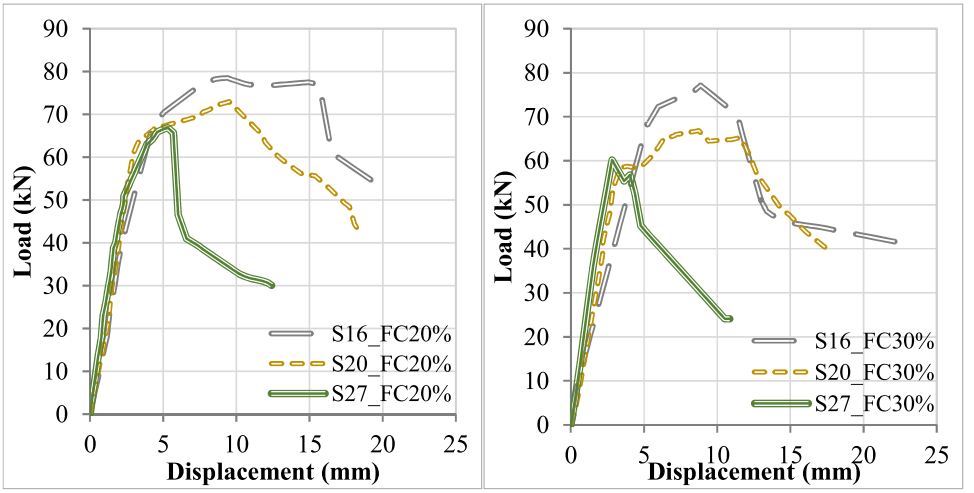


**Fig. 17.** Comparison of load displacement of RCBs for 20 % and 30 % WFC ratio with stirrup spacing; a) 160 mm, b) 200 mm, c) 270 mm.

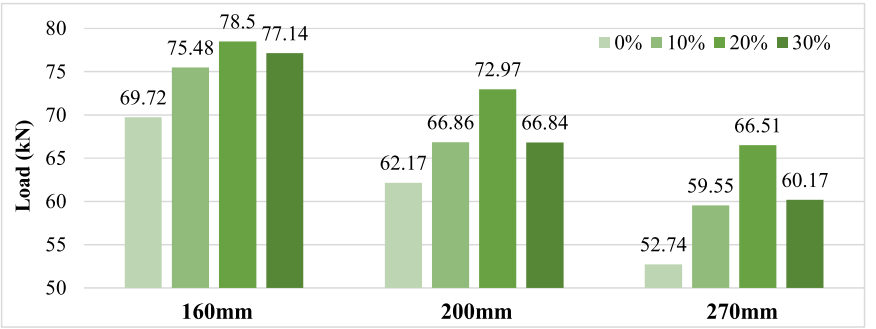


**Fig. 18.** Comparison of load displacement of RCBs for altered WFC ratio with stirrup spacing.

Finally, observe of WFC is selected as 0 %, 10 %, 20 %, and 30 % while stirrup spacing in the RCB is selected continuously as 270 mm. As observed by investigational tests consequences for 0 %, 10 %, 20 % and 30 %, it is observed that there were not bending cracks in the RCB depending on the vertical load as offered in Figs. 24 and 25. According to Fig. 24, Φ27_FC20 %, the specimen has the most load-bearing ability. In other words, it has a 23.8 %, 12.3 % and 11.1 % more load-carrying ability than specimens with a WFC content of 0 %, 10 %, and 30 %, respectively. The maximum load-bearing ability was observed for 20 % WFC. As the load-displacement curve was observed, the deformation improved linearly with increasing loading. A significant reduction was observed as the WFC addition level was greater than 20 % as presented in Fig. 24. All of the specimens reached collapse mode with DT collapse damage. Concrete damage was also observed with the leverage influence in specimens other than the Φ27_FC30 % specimen.

Altered WFC percentages with stirrup spacing are collated in Fig. 26. The changes in load, displacement, stiffness, ductility, and energy dissipation capacities obtained from experimental studies are given in Tables 7 and 8.

### *3.2.4. Comparison of shear test consequences with ACI 318 codes*

In the study, the equations recommended in the ACI 318–19 regulation were used to determine the shear strength of the RCBs. ACI 318–19 proposed a method in which the contribution of concrete ($V_c$) and stirrups ($V_s$) to the shear strength are considered together in the calculation of shear ability (Eq. 10). Eq. 8 was used in the calculation of the shear ability since it is considered that the concrete contributes to the shear ability together with the longitudinal reinforcement and that the minimum stirrup area is provided. In addition, the contribution of stirrups to shear ability was calculated using Eq. 9.

$$V_c = 0.66\lambda\sqrt[3]{\rho_w}\sqrt{f'_c}b_w d \le 0.42\lambda\sqrt{f'_c}b_w dA_v \ge A_{v,\min} = 0.062\sqrt{f'_c}\frac{b_w}{f_{yt}}sA_v \ge A_{v,\min} = 0.35\frac{b_w}{f_{yt}}s \tag{8}$$

$$V_s = \frac{A_w f_{yt}}{s}d \le 0.66\sqrt{f'_c}b_w d \tag{9}$$

$$V_n = V_c + V_s \tag{10}$$

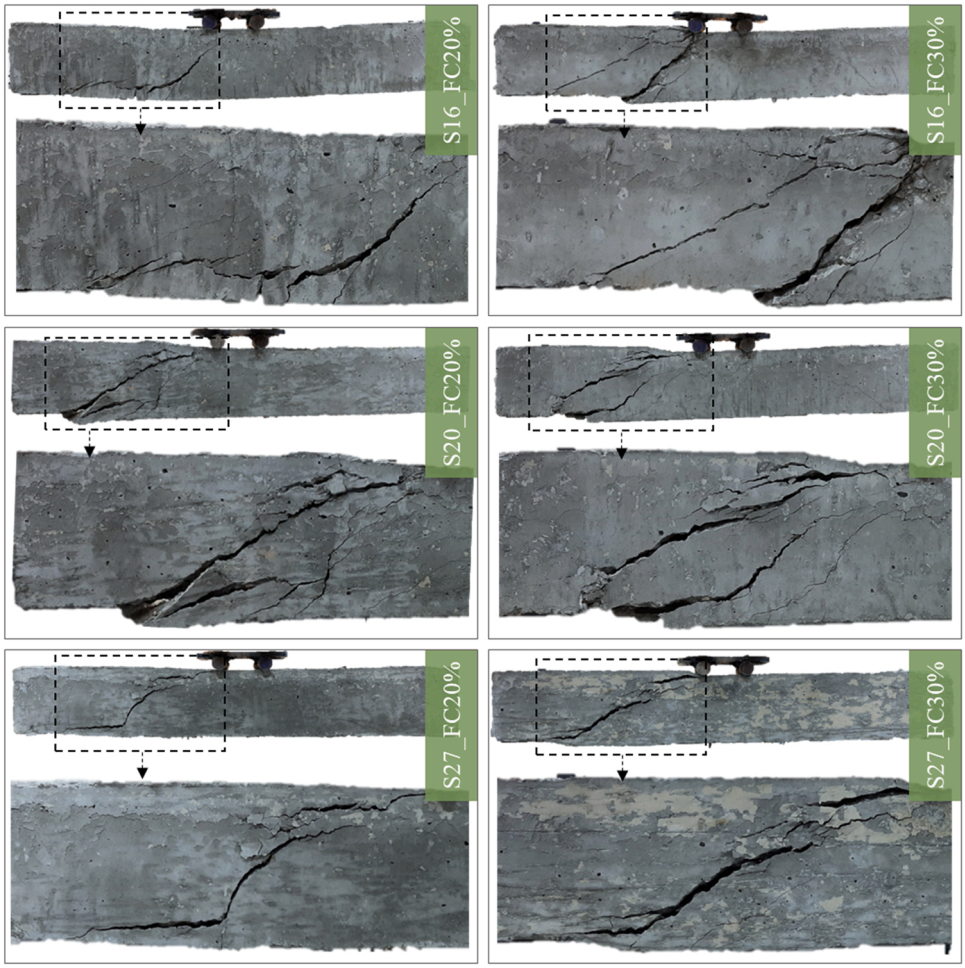


**Fig. 19.** Comparison of collapse patterns for 20 % and 30 % WFC ratio with stirrup spacing a) 160 mm, b) 200 mm, c) 270 mm.

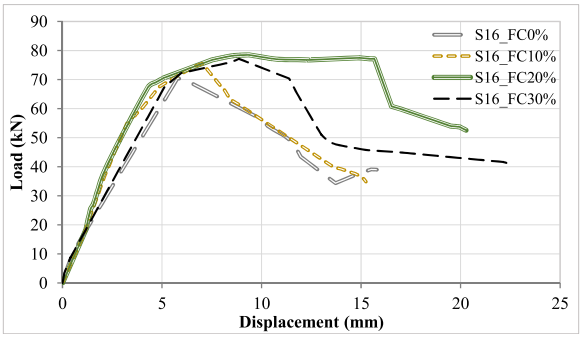


**Fig. 20.** Comparison of load displacement of RCBs with stirrup spacing 160 mm for a altered amount of WFC.

$\lambda$ is the modification factor of concrete (1 for normal weight concrete), $\rho_w$ is the tensile reinforcement ratio ($mm^2$), $A_w$ is the shear reinforcement area ($mm^2$), $s$ is the center to center spacing of shear reinforcement (mm), $f_{yt}$ is the shear reinforcement yield strength (MPa).

Experimental shear strengths and shear strengths of RCBs according to ACI 318–19 are presented in Table 9. As can be noted in the table, there is a maximum difference of 10 % amid the calculated shear strengths of non-FC added RCBs and the test consequences. However, as the stirrup spacing decreased, this difference decreased considerably as the shear crack coincided with at least one stirrup and the shear force was carried by the stirrup, and the difference decreased to 1 %. In FC reinforced RCBs, the difference amid the

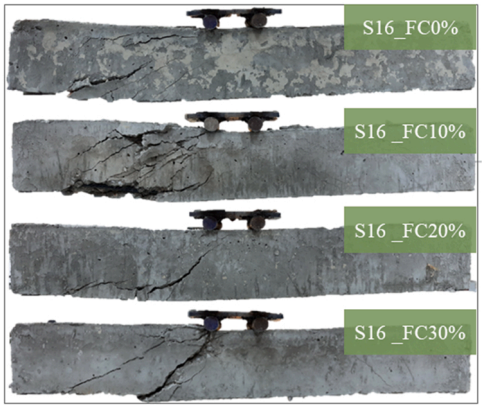


**Fig. 21.** Comparison of load displacement of RCBs with stirrup spacing 160 mm a) 0 %, b) 10 %, c) 20 % and d) 30 % WFC percentages.

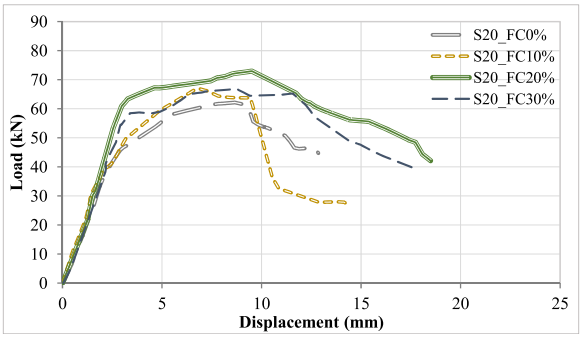


**Fig. 22.** Comparison of load displacement of RCBs with stirrup spacing 200 mm for a altered amount of WFC.

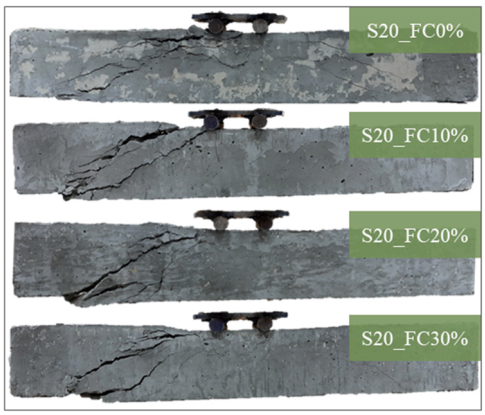


**Fig. 23.** Comparison of load displacement of RCBs with stirrup spacing 200 mm a) 0 %, b) 10 %, c) 20 % and d) 30 % WFC percentages.

calculated shear strengths and the experimental shear strengths decreases as the stirrup spacing decreases. However, as the FC contribution amount increased, the differences amid the calculation consequences and the experimental consequences became wider. These differences were up to 32 % in the 270 mm stirrup range, up to 19 % in the 200 mm stirrup range, and up to 10 % in the 160 mm stirrup range. This situation gives the impression that the use of FC additive in the concrete combination, especially up to 20 %, in the first stage, increases the tensile strength of the concrete and the concrete resists the principal tensile stresses more. However, this situation is reflected in the equation with the expression of the square root of the concrete CS in the shear equation. In addition, the differences amid the splitting test consequences are insufficient to fully describe this situation. So, it can be argued that this difference is due to FC additive's improvement in concrete-reinforcement adherence. Because, as can be realized especially when Figs. 22 and 23 are observed, the stiffness of the beam was preserved until the first major crack by increasing the FC contribution up to 20 %. This was

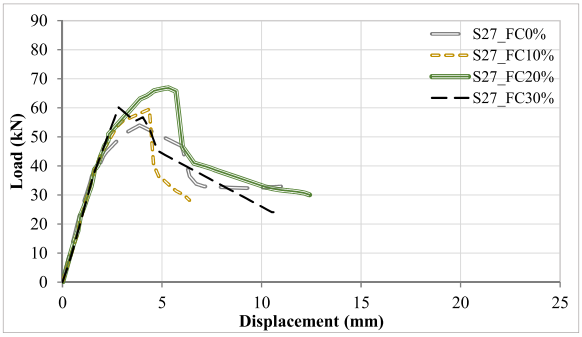


**Fig. 24.** Comparison of load displacement of RCBs with stirrup spacing 270 mm for a altered amount of WFC.

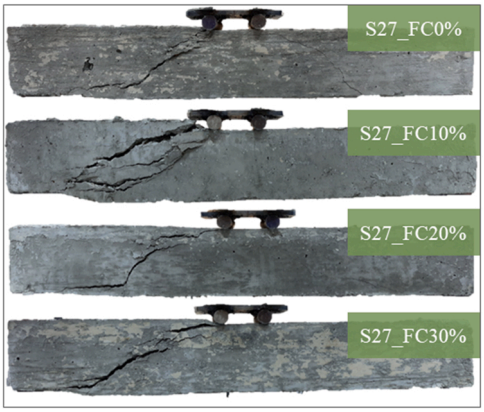


**Fig. 25.** Comparison of load displacement of RCBs with stirrup spacing 270 mm a) 0 %, b) 10 %, c) 20 %, and d) 30 % WFC percentages.

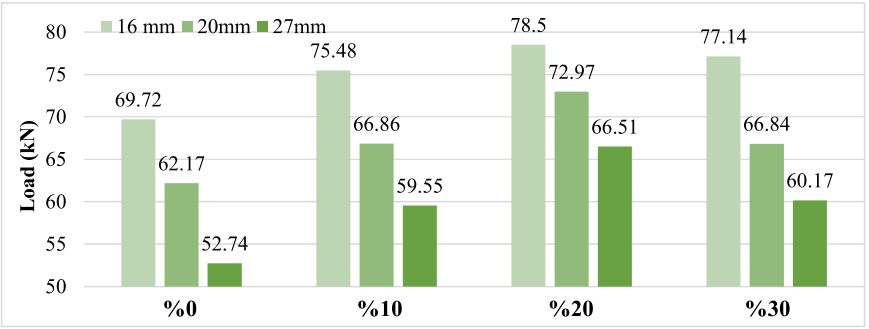


**Fig. 26.** Comparison for altered WFC ratio with stirrup spacing.

due to the delay in stripping of stirrups as their adherence to concrete increased. For this reason, the calculated shear strengths of the 20 % FC reinforced RCBs were found to be quite low collated to the experimental consequences.

## 4. Conclusion

This investigational research study considered the belongings of altered quantities of WFC ratio on the shear and bending performance of RCBs using altered stirrup spacing. The investigational study consequences were collated. The consequences established as a consequence of the study are brief as follows:

- WFC can be used instead of FAs at altered rates. While the WFC content for bending RCBs increases the ability at the maximum level for the range of 20 %−30 %, it can be said that the optimum WFC content for shear RCBs is 20 %.

**Table 7**
Experimental consequences for load and displacement values.

| Test specimens | $P_{max}$ (kN) | Displacement at $P_{max}$ (mm) | Stiffness at ($P_{max}$) (kN/mm) | $P_u$ (*0.85* $P_{max}$) (kN) | Displacement at Yield $\delta_y$ (mm) | Stiffness at Yield (kN/mm) | $\delta_u$ (mm) | Ductility ratio |
|---|---|---|---|---|---|---|---|---|
| Φ27_FC0 % | 54.00 | 3.86 | 13.95 | 45.90 | 2.35 | 19.51 | 6.03 | 2.56 |
| Φ20_FC0 % | 62.17 | 8.65 | 7.18 | 52.84 | 4.45 | 11.86 | 10.48 | 2.35 |
| Φ16_FC0 % | 70.54 | 5.79 | 12.18 | 59.96 | 4.86 | 12.32 | 8.97 | 1.84 |
| Φ27_FC10 % | 59.54 | 4.36 | 13.64 | 50.61 | 2.48 | 20.35 | 4.46 | 1.79 |
| Φ20_FC10 % | 66.86 | 6.90 | 9.68 | 56.83 | 4.48 | 12.66 | 9.73 | 2.16 |
| Φ16_FC10 % | 75.48 | 7.03 | 10.73 | 64.16 | 4.46 | 14.37 | 8.33 | 1.86 |
| Φ27_FC20 % | 66.87 | 5.31 | 12.58 | 56.84 | 3.08 | 18.40 | 5.85 | 1.89 |
| Φ20_FC20 % | 72.97 | 9.50 | 7.67 | 62.03 | 3.11 | 19.93 | 12.42 | 3.99 |
| Φ16_FC20 % | 78.50 | 9.38 | 8.36 | 66.72 | 4.15 | 16.05 | 16.21 | 3.90 |
| Φ27_FC30 % | 60.16 | 2.81 | 21.35 | 51.14 | 2.32 | 21.99 | 4.45 | 1.91 |
| Φ20_FC30 % | 66.84 | 8.74 | 7.64 | 56.81 | 3.21 | 17.69 | 12.74 | 3.96 |
| Φ16_FC30 % | 77.14 | 8.86 | 8.69 | 65.57 | 4.97 | 13.17 | 11.75 | 2.36 |

**Table 8**
Experimental test consequences for energy dissipation capacities.

| Test specimens | Maximum Displacement (mm) | Energy Dissipation at $P_{max}$ (kJ) | Energy Dissipation at *0.85* $P_{max}$ (kJ) | Plastic Energy Dissipation (kJ) | Total Energy Dissipation (kJ) | Collapse type |
|---|---|---|---|---|---|---|
| Φ27_FC0 % | 10.97 | 0.248 | 0.078 | 0.337 | 0.416 | Shear |
| Φ20_FC0 % | 12.84 | 0.436 | 0.168 | 0.447 | 0.615 | Shear |
| Φ16_FC0 % | 15.79 | 0.235 | 0.231 | 0.497 | 0.729 | Shear |
| Φ27_FC10 % | 6.37 | 0.186 | 0.085 | 0.161 | 0.246 | Shear |
| Φ20_FC10 % | 14.27 | 0.329 | 0.270 | 0.371 | 0.641 | Shear |
| Φ16_FC10 % | 15.24 | 0.412 | 0.221 | 0.549 | 0.770 | Shear |
| Φ27_FC20 % | 12.40 | 0.270 | 0.162 | 0.354 | 0.516 | Shear |
| Φ20_FC20 % | 18.49 | 0.687 | 0.116 | 0.942 | 1.059 | Bending+Shear |
| Φ16_FC20 % | 20.27 | 0.619 | 0.171 | 1.119 | 1.290 | Bending+Shear |
| Φ27_FC30 % | 10.85 | 0.136 | 0.116 | 0.288 | 0.404 | Shear |
| Φ20_FC30 % | 17.76 | 0.480 | 0.117 | 0.811 | 0.929 | Bending+Shear |
| Φ16_FC30 % | 22.52 | 0.642 | 0.191 | 0.975 | 1.165 | Shear |

**Table 9**
Comparison of experimental consequences with ACI 318–19.

| Exp. | *fc'* | $V_{c,ACI}$ | $V_{s,ACI}$ | $V_{n,ACI}$ | $V_{Exp.}$ | $V_{Exp.}/V_{n,ACI}$ | Exp. | *fc'* | $V_{c,ACI}$ | $V_{s,ACI}$ | $V_{n,ACI}$ | $V_{Exp.}$ | $V_{Exp.}/V_{n,ACI}$ |
|---|---|---|---|---|---|---|---|---|---|---|---|---|---|
| Φ27_FC0 | 17.7 | 9.4 | 15.2 | 24.6 | 27.0 | 1.10 | Φ27_FC20 | 20.4 | 10.0 | 15.2 | 25.3 | 33.4 | 1.32 |
| Φ20_FC0 | 17.7 | 9.4 | 20.6 | 29.9 | 31.1 | 1.04 | Φ20_FC20 | 20.4 | 10.0 | 20.6 | 30.7 | 36.9 | 1.19 |
| Φ16_FC0 | 17.7 | 9.4 | 25.7 | 35.1 | 35.3 | 1.01 | Φ16_FC20 | 20.4 | 10.0 | 25.7 | 35.8 | 39.3 | 1.10 |
| Φ27_FC10 | 18.8 | 9.6 | 15.2 | 24.9 | 29.8 | 1.20 | Φ27_FC30 | 18.3 | 9.5 | 15.2 | 2.5 | 30.1 | 1.22 |
| Φ20_FC10 | 18.8 | 9.6 | 20.6 | 30.2 | 33.4 | 1.11 | Φ20_FC30 | 18.3 | 9.5 | 20.6 | 30.1 | 33.4 | 1.11 |
| Φ16_FC10 | 18.8 | 9.6 | 25.7 | 35.4 | 37.7 | 1.07 | Φ16_FC30 | 18.3 | 9.5 | 25.7 | 35.2 | 38.6 | 1.09 |

- While bending+shear collapse was observed in all WFC RCBs with a longitudinal tensile reinforcement ratio of Φ12 in bending RCBs, only bending collapse was observed in all WFC RCBs with Φ10 and Φ8.
- Increasing the tensile reinforcement ratio has made the WFC less effective. Similarly, as stirrup spacing decreases, stirrup dominates the behavior, and as stirrup spacing increases, WFC determines the behavior.
- As the stirrup reinforcement spacing decreased in shear RCBs, total energy consumption increased. Besides, it is assumed that there is a linear correlation amid the rise in the WFC content and the rise in the total energy depletion ability.
- In RCBs with stirrups and an a/d ratio of around 2.5, common damage is DT and SC collapse. When all shear RCBs were evaluated, SC collapse was observed only in Φ16_FC0 %, Φ16_FC20 % and Φ20_FC0 % specimens, while DT collapse was observed in all other specimens. In addition, concrete damages were observed in Φ16_FC20 %, Φ20_FC30 %, Φ27_FC0 %, Φ27_FC10 %, Φ27_FC20 % specimens due to the leverage influence.
- Maximum of 10 % difference was detected amid the actual and expected values by ACI 318 for the RCBs failed due shear or bending.

As a result of bending and shear beam tests, WFC can be used for recycling in concrete at a specific rate. It is crucial to obtain analytical formulas in future studies. In this way, the design formulas for the 20 %−30 % determined for WFC will contribute for the

researchers.

## Declaration of Competing Interest

The authors declare that they have no known competing financial interests or personal relationships that could have appeared to influence the work reported in this paper.

## Data Availability

Data will be made available on request.

## Acknowledgments

This study had support by the Conselho Nacional de Desenvolvimento Científico e Tecnológico (CNPq), Project n. 408498/2022-6, Brazil.

## References

[1] U. Javed, R.A. Khushnood, S.A. Memon, F.E. Jalal, M.S. Zafar, Sustainable incorporation of lime-bentonite clay composite for production of ecofriendly bricks, J. Clean. Prod. 263 (2020), 121469.
[2] X. Lingling, G. Wei, W. Tao, Y. Nanru, Study on fired bricks with replacing clay by fly ash in high volume ratio, Constr. Build. Mater. 19 (2005) 243–247.
[3] M. Samadi, G.F. Huseien, H. Mohammadhosseini, H-s. Lee, N.H.A.S. Lim, M.M.D. Tahir, et al., Waste ceramic as low cost and eco-friendly materials in the production of sustainable mortars, J. Clean. Prod. 266 (2020), 121825.
[4] Ö. Zeybek, Y.O. Özkılıç, M. Karalar, A.İ. Çelik, S. Qaidi, J. Ahmad, et al., Influence of replacing cement with waste glass on mechanical properties of concrete 15 (2022) 7513.
[5] Ö. Zeybek, Y.O. Özkılıç, et al., Performance evaluation of fiber-reinforced concretes produced with steel fibers extracted from waste tire, Front. Mater. (2022).
[6] S. Qaidi, H.M. Najm, S.M. Abed, Y.O. Özkılıç, H. Al Dughaishi, M. Alosta, et al., Concrete containing waste glass as an environmentally friendly aggregate: a review on fresh and mechanical characteristics 15 (2022) 6222.
[7] R. Martínez-García, P. Jagadesh, O. Zaid, A.A. Şerbănoiu, F.J. Fraile-Fernández, J. de Prado-Gil, et al., The present state of the use of waste wood ash as an eco-efficient construction material: a review, Materials 15 (2022) 5349.
[8] M. Karalar, Y.O. Özkılıç, A.F. Deifalla, C. Aksoylu, M.H. Arslan, M. Ahmad, et al., Improvement in bending performance of reinforced concrete beams produced with waste lathe scraps 14 (2022) 12660.
[9] M. Karalar, Y.O. Özkılıç, C. Aksoylu, M.M.S. Sabri, N.B. Alexey, et al., Flexural behavior of reinforced concrete beams using waste marble powder towards application of sustainable concrete, Front. Mater. (2022).
[10] M. Karalar, T. Bilir, M. Çavuşlu, Y.O. Özkılıç, M.M.S. Sabri, Use of recycled coal bottom ash in reinforced concrete beams as replacement for aggregate (2022), 1064604.
[11] M.A. El-Mandouh, J.-W. Hu, A.S. Mohamed, A.S. Abd El-Maula, Assessment of waste marble powder on the mechanical properties of high-strength concrete and evaluation of its shear strength, Materials 15 (2022) 7125.
[12] B. Basaran, I. Kalkan, C. Aksoylu, Y.O. Özkılıç, M.M.S. Sabri, Effects of waste powder, fine and coarse marble aggregates on concrete compressive strength 14 (2022) 14388.
[13] C. Aksoylu, Y.O. Özkılıç, M. Hadzima-Nyarko, E. Işık, M.H. Arslan, Investigation on improvement in shear performance of reinforced-concrete beams produced with recycled steel wires from waste tires 14 (2022) 13360.
[14] F. Fiol, V. Revilla-Cuesta, C. Thomas, J.M. Manso, Self-compacting concrete containing coarse recycled precast-concrete aggregate and its durability in marine-environment-related tests, Constr. Build. Mater. 377 (2023), 131084.
[15] X.-Y. Zhao, J.-X. Chen, G.-M. Chen, J.-J. Xu, L.-W. Zhang, Prediction of ultimate condition of FRP-confined recycled aggregate concrete using a hybrid boosting model enriched with tabular generative adversarial networks, Thin-Walled Struct. 182 (2023), 110318.
[16] J. Xu, W. Xiong, X. Guo, T. Lai, Y. Liu, W. Ying, Properties of using excavated soil waste as fine and coarse aggregates in unfired clay bricks after dry-wet cycles, Case Stud. Constr. Mater. 17 (2022), e01471.
[17] M. Sahu, L. Singh, Critical review on types of bricks type 13: wood ash bricks, Int. J. Mech. Prod. Eng. 5 (2017) 80–83.
[18] S.M.S. Kazmi, M.J. Munir, I. Patnaikuni, Y.-F. Wu, U. Fawad, Thermal performance enhancement of eco-friendly bricks incorporating agro-wastes, Energy Build. 158 (2018), 1117-29.
[19] S. Fayed, E. Madenci, Y.O. Özkiliç, W. Mansour, Improving bond performance of ribbed steel bars embedded in recycled aggregate concrete using steel mesh fabric confinement, Constr. Build. Mater. 369 (2023), 130452.
[20] Celik Aİ, Y.O. Özkılıç, Geopolymer concrete with high strength, workability and setting time using recycled steel wires and basalt powder, STEEL COMPOSITE Struct. 46 (2023) 689–707.
[21] M.C. Acar, A.İ. Çelik, R. Kayabaşı, A. Şener, N. Özdöner, Y.O. Özkılıç, Production of perlite-based-aerated geopolymer using hydrogen peroxide as eco-friendly material for energy-efficient buildings, J. Mater. Res. Technol. 24 (2023) 81–99.
[22] E.M. Shcherban', S.A. Stel'makh, A.N. Beskopylny, L.R. Mailyan, B. Meskhi, A.A. Shilov, et al., Normal-weight concrete with improved stress–strain characteristics reinforced with dispersed coconut fibers, Appl. Sci. 12 (2022) 11734.
[23] R.G. de Azevedo, A. Amin, M. Hadzima-Nyarko, M. Saad Agwa, I. Zeyad, A.M. Tayeh, et al., Possibilities for the application of agro-industrial wastes in cementitious materials: a brief review of the Brazilian perspective, Clean. Mater. 3 (2022), 100040.
[24] E. Madenci, S. Fayed, W. Mansour, Y.O. Ozkilic, Buckling performance of pultruded glass fiber reinforced polymer profiles infilled with waste steel fiber reinforced concrete under axial compression, Steel Composite Struct. 45 (2022) 653–663.
[25] A.R.G. de Azevedo, M.T. Marvila, M.A.B. de Oliveira, C.E.M. Umbuzeiro, N.R.C. Huaman, S.N. Monteiro, Perspectives for the application of bauxite wastes in the development of alternative building materials, J. Mater. Res. Technol. 20 (2022), 3114-25.
[26] A.İ. Çelik, Y.O. Özkılıç, Ö. Zeybek, N. Özdöner, B.A. Tayeh, Performance assessment of fiber-reinforced concrete produced with waste lathe fibers 14 (2022) 11817.
[27] A.N. Beskopylny, et al., Composition component influence on concrete properties with the additive of rubber tree seed shells, . Appl. Sci. 12 (2022) 11744.
[28] F. Aslam, O. Zaid, F. Althoey, S.H. Alyami, S.M.A. Qaidi, J. de Prado Gil, et al., Evaluating the influence of fly ash and waste glass on the characteristics of coconut fibers reinforced concrete, Struct. Concr. (2022).
[29] M.M. Arbili, M. Alqurashi, A. Majdi, J. Ahmad, A.F. Deifalla, Concrete made with iron ore tailings as a fine aggregate: a step towards sustainable concrete, Materials 15 (2022) 6236.
[30] A.A. Alani, R. Lesovik, V. Lesovik, R. Fediuk, S. Klyuev, M. Amran, et al., Demolition waste potential for completely cement-free binders, Materials 15 (2022) 6018.

[31] J. Ahmad, R. Martinez-Garcia, S. Algarni, J. de-Prado-Gil, T. Alqahtani, K. Irshad, Characteristics of sustainable concrete with partial substitutions of glass waste as a binder material, Int. J. Concr. Struct. Mater. 16 (2022) 1–18.
[32] W. Mansour, S. Fayed, Flexural rigidity and ductility of RC beams reinforced with steel and recycled plastic fibers, Steel Compos. Struct. 41 (2021) 317–334.
[33] A. İssi, N. Derin Coşkun, V. Tiryaki, V. Uz, Casting and sintering of a sanitaryware body containing fine fire clay (FFC), J. Aust. Ceram. Soc. 53 (2017), 157-62.
[34] P. Joyklad, A. Nawaz, Q. Hussain, Effect of fired clay brick aggregates on mechanical properties of concrete, Suranaree J. Sci. Technol. (2018) 25.
[35] M.J. Miah, M.M.H. Patoary, S.C. Paul, A.J. Babafemi, B. Panda, Enhancement of mechanical properties and porosity of concrete using steel slag coarse aggregate, Materials 13 (2020) 2865.
[36] J.P. Zachariah, P.P. Sarkar, D. Nandi, A study on the properties of cement grouted open-graded bituminous concrete with brick as aggregates, Constr. Build. Mater. 256 (2020), 119436.
[37] T. Manzur, R.S. Huq, I.H. Efaz, S. Afroz, F. Rahman, K. Hossain, Performance enhancement of brick aggregate concrete using microbiologically induced calcite precipitation, Case Stud. Constr. Mater. 11 (2019), e00248.
[38] M.J. Miah, M. Ali, Y. Li, A.J. Babafemi, S.C. Paul, Impact of induction furnace steel slag as replacement for fired clay brick aggregate on flexural and durability performances of RC beams, Materials 14 (2021) 6268.
[39] C. Zheng, C. Lou, G. Du, X. Li, Z. Liu, L. Li, Mechanical properties of recycled concrete with demolished waste concrete aggregate and clay brick aggregate, Results Phys. 9 (2018), 1317-22.
[40] N.M. Ibrahim, S. Salehuddin, R.C. Amat, N.L. Rahim, T.N.T. Izhar, Performance of lightweight foamed concrete with waste clay brick as coarse aggregate, Apcbee Procedia 5 (2013) 497–501.
[41] S. Zhang, P. He, L. Niu, Mechanical properties and permeability of fiber-reinforced concrete with recycled aggregate made from waste clay brick, J. Clean. Prod. 268 (2020), 121690.